The Astrophysical Journal, 732:121 (13pp), 2011 May 10 doi:10.1088/0004-637X/732/2/121
© 2011. The American Astronomical Society. All rights reserved. Printed in the U.S.A.

BROAD-LINE REVERBERATION IN THE *KEPLER*-FIELD SEYFERT GALAXY Zw 229-015

Aaron J. Barth[1], My L. Nguyen[1], Matthew A. Malkan[2], Alexei V. Filippenko[3], Weidong Li[3], Varoujan Gorjian[4], Michael D. Joner[5], Vardha Nicola Bennert[6], Janos Botyanszki[7], S. Bradley Cenko[3], Michael Childress[7], Jieun Choi[3], Julia M. Comerford[8], Antonino Cucciara[7], Robert da Silva[9], Gaspard Duchêne[3,10], Michele Fumagalli[11], Mohan Ganeshalingam[3], Elinor L. Gates[12], Brian F. Gerke[13], Christopher V. Griffith[14], Chelsea Harris[6], Eric G. Hintz[5], Eric Hsiao[7], Michael T. Kandrashoff[3], William C. Keel[15], David Kirkman[16], Io K. W. Kleiser[3], C. David Laney[5], Jeffrey Lee[16], Liliana Lopez[16], Thomas B. Lowe[12], J. Ward Moody[5], Alekzandir Morton[3], A. M. Nierenberg[6], Peter Nugent[3,7], Anna Pancoast[6], Jacob Rex[3], R. Michael Rich[2], Jeffrey M. Silverman[3], Graeme H. Smith[9], Alessandro Sonnenfeld[6], Nao Suzuki[7], David Tytler[16], Jonelle L. Walsh[1], Jong-Hak Woo[17], Yizhe Yang[18], and Carl Zeisse[16]

[1] Department of Physics and Astronomy, 4129 Frederick Reines Hall, University of California, Irvine, CA 92697-4575, USA; barth@uci.edu
[2] Department of Physics and Astronomy, University of California, Los Angeles, CA 90024, USA
[3] Department of Astronomy, University of California, Berkeley, CA 94720-3411, USA
[4] Jet Propulsion Laboratory, 4800 Oak Grove Boulevard, MS 169-327, Pasadena, CA 91109, USA
[5] Department of Physics and Astronomy, N283 ESC, Brigham Young University, Provo, UT 84602-4360, USA
[6] Department of Physics, University of California, Santa Barbara, CA 93106, USA
[7] Lawrence Berkeley National Laboratory, 1 Cyclotron Road, Berkeley, CA 94720, USA
[8] Astronomy Department, University of Texas at Austin, Austin, TX 78712, USA
[9] University of California Observatories/Lick Observatory, Santa Cruz, CA 95064, USA
[10] UJF-Grenoble 1/CNRS-INSU, Institut de Planétologie et d'Astrophysique de Grenoble (IPAG) UMR 5274, Grenoble F-38041, France
[11] Department of Astronomy and Astrophysics, University of California, Santa Cruz, CA 95064, USA
[12] Lick Observatory, P.O. Box 85, Mount Hamilton, CA 95140, USA
[13] Kavli Institute for Particle Astrophysics and Cosmology, SLAC National Accelerator Laboratory, 2575 Sand Hill Rd., M/S 29, Menlo Park, CA 94025, USA
[14] Department of Astronomy and Astrophysics, The Pennsylvania State University, 525 Davey Lab, University Park, PA 16802, USA
[15] Department of Physics and Astronomy, University of Alabama, P.O. Box 870324, Tuscaloosa, AL 35487, USA
[16] Center for Astrophysics and Space Sciences, University of California, San Diego, CA 92093-0424, USA
[17] Astronomy Program, Department of Physics and Astronomy, Seoul National University, Seoul 151-742, Republic of Korea
[18] Department of Physics and Department of Mathematics, University of California, Berkeley, CA 94720, USA
Received 2011 January 22; accepted 2011 March 10; published 2011 April 26

ABSTRACT

The Seyfert 1 galaxy Zw 229-015 is among the brightest active galaxies being monitored by the *Kepler* mission. In order to determine the black hole mass in Zw 229-015 from Hβ reverberation mapping, we have carried out nightly observations with the Kast Spectrograph at the Lick 3 m telescope during the dark runs from 2010 June through December, obtaining 54 spectroscopic observations in total. We have also obtained nightly *V*-band imaging with the Katzman Automatic Imaging Telescope at Lick Observatory and with the 0.9 m telescope at the Brigham Young University West Mountain Observatory over the same period. We detect strong variability in the source, which exhibited more than a factor of two change in broad Hβ flux. From cross-correlation measurements, we find that the Hβ light curve has a rest-frame lag of $3.86^{+0.69}_{-0.90}$ days with respect to the *V*-band continuum variations. We also measure reverberation lags for Hα and Hγ and find an upper limit to the Hδ lag. Combining the Hβ lag measurement with a broad Hβ width of $\sigma_{\rm line} = 1590 \pm 47$ km s^{-1} measured from the rms variability spectrum, we obtain a virial estimate of $M_{\rm BH} = 1.00^{+0.19}_{-0.24} \times 10^7\ M_\odot$ for the black hole in Zw 229-015. As a *Kepler* target, Zw 229-015 will eventually have one of the highest-quality optical light curves ever measured for any active galaxy, and the black hole mass determined from reverberation mapping will serve as a benchmark for testing relationships between black hole mass and continuum variability characteristics in active galactic nuclei.

Key words: galaxies: active – galaxies: individual (Zw 229-015) – galaxies: nuclei

Online-only material: color figures, machine-readable tables

1. INTRODUCTION

The NASA *Kepler* mission (Borucki et al. 2010a) is designed to search for exoplanets by detecting transit events, and early results have demonstrated the spectacular quality of *Kepler*'s ultra-precise photometry (e.g., Borucki et al. 2010b). In addition to its primary goal of obtaining light curves of Galactic stars, *Kepler* is monitoring a small number of active galactic nuclei (AGNs) of various types, including Seyfert galaxies, quasars, and blazars. *Kepler* will provide the best optical light curves ever obtained of AGNs, vastly exceeding the quality of any previous observations in terms of both sampling cadence and photometric accuracy. This will enable unprecedented measurements of the characteristic properties of AGN optical variability.

One of the key motivations for the measurement of high-precision AGN light curves is to determine the power spectrum of continuum fluctuations and to search for any characteristic timescales of variability (in the form of breaks or slope changes in the power spectrum of variations), which might be related to light-crossing, dynamical, or thermal timescales in the accretion disk. At X-ray energies, long-duration light curves have been used to search for breaks in the power spectral density (e.g., Uttley et al. 2002; Markowitz et al. 2003), and the break timescales are observed to be dependent on both black hole mass

and luminosity across a range extending from X-ray binaries to quasars (McHardy et al. 2006). There is accumulating evidence that the optical fluctuations of AGNs also contain characteristic timescales that may depend on black hole mass and luminosity (Collier & Peterson 2001; Kelly et al. 2009; MacLeod et al. 2010).

Ground-based optical light curves of AGNs are limited in quality by nightly and seasonal sampling, weather, and seeing-dependent errors, but *Kepler* can provide exquisite data that will for the first time enable detailed measurements of the optical variability properties of individual objects over timescales ranging from hours up to (potentially) a few years. Unobscured (Type 1) AGNs monitored by *Kepler* can provide powerful tests of proposed relationships between variability properties, black hole mass, and luminosity that have been derived from larger samples of objects with lower-quality ground-based light curves.

In order to fully exploit the results of these *Kepler* AGN observations, independent measurements of black hole masses in *Kepler*-field AGNs are needed. Here, we present the results of a six-month, ground-based, optical reverberation-mapping program for the *Kepler* target Zw 229-015 (at $z = 0.0275$; Falco et al. 1999), with the goal of determining the black hole mass in this galaxy from its Hβ reverberation lag.

This galaxy (also known as CGCG 229-015 or 2MASX J19052592+4227398) was first identified as a Type 1 Seyfert by Proust (1990). Since then, no follow-up observations of this AGN have been reported in the literature at all, aside from its inclusion in *ROSAT* All-Sky Survey source catalogs (Voges et al. 1999; Zimmermann et al. 2001). Nevertheless, Zw 229-015 is one of the nearest and brightest AGNs in the *Kepler* field, and it was selected as a monitoring target for the first two cycles of *Kepler* observations. To assess its suitability for ground-based monitoring, we obtained a test spectroscopic exposure at the Lick Observatory 3 m Shane telescope in 2010 April. This observation reconfirmed the Seyfert 1 classification, and we then selected it for the reverberation-mapping program reported here. In this paper, we describe our imaging and spectroscopic observations of Zw 229-015, the measurements of the continuum and emission-line light curves and the broad emission-line reverberation lag, and an estimate of the black hole mass based on the Hβ lag and line width.

2. IMAGING OBSERVATIONS

Reverberation measurements require a light curve of the AGN continuum, and we obtained *V*-band photometry of Zw 229-015 following the same strategy used in recent reverberation programs (e.g., Walsh et al. 2009; Denney et al. 2010). Although ground-based measurements cannot approach the accuracy or sampling cadence of the *Kepler* data, they allowed us to monitor the target's variability continuously during the course of our observing program. Furthermore, the *V*-band photometry gives a nearly line-free measurement of the galaxy's continuum flux, while the broad *Kepler* spectral response includes the Hα and Hβ lines from the AGN.

We obtained regularly scheduled *V*-band imaging at the 0.76 m Katzman Automatic Imaging Telescope (KAIT) at Lick Observatory, and at the 0.9 m telescope at the Brigham Young University West Mountain Observatory (WMO). At both telescopes, Zw 229-015 was observed each night during the monitoring period, except when precluded by weather or instrument problems. We also obtained a small number of images at other facilities, as described below. Figure 1 illustrates the field surrounding Zw 229-015. The galaxy has a barred spiral morphology, with a Hubble type of roughly SBa.

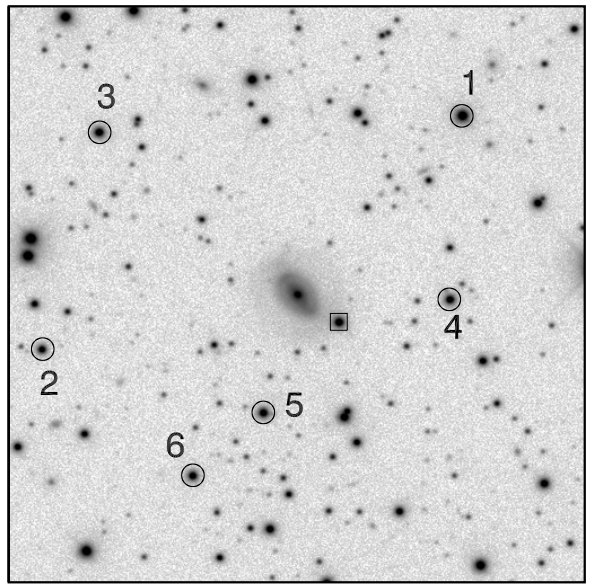

Figure 1. *V*-band image centered on Zw 229-015, created by stacking the 18 best-seeing frames (all with seeing better than 1″.5) from the West Mountain Observatory. North is up and east to the left, and the size of the displayed region is 250″ × 250″. Photometric comparison stars are circled and labeled, and the star that fell in the spectroscopic aperture is marked with a square.

2.1. KAIT

The KAIT 0.76 m robotic telescope (Filippenko et al. 2001) uses a 512 × 512 pixel SITe CCD camera with a scale of 0″.8 pixel^{-1}. A single 300 s exposure of Zw 229-015 was obtained on each night, weather permitting, from June 3 through December 13 (UT dates are used throughout this paper). During the monitoring period, KAIT had two-month-long shutdowns for repairs, first in August and again from mid-October to mid-November. The median seeing for all KAIT exposures was 2″.15. The automatic KAIT data-processing pipeline includes bias subtraction and flat fielding.

2.2. West Mountain Observatory

The 0.9 m telescope at the WMO is one of five small research telescopes operated by Brigham Young University. It was installed and tested in late 2009 and began working in a partially queue-scheduled mode during the 2010 observing season. The observations secured for this investigation were scheduled as part of an external guest investigator program.

From June 5 until September 1, observations were made using a 3056 × 3056 pixel KAF 09000 CCD camera with a scale of 0″.5 pixel^{-1}. After September 2, observations were made using a 2048 × 2048 pixel Fairchild 3041-UV CCD camera with a scale of 0″.6 pixel^{-1}. The typical observing procedure was to secure two exposures of Zw 229-015 while it was close to meridian transit on each night that conditions permitted telescope operations. Exposures were 300 s from the start of monitoring until September 7 and were decreased to 200 s thereafter because of the higher sensitivity of the Fairchild CCD. Observations continued until December 13, but only a few exposures were obtained after November 5 due to poor weather. Standard-star fields from Landolt (1992) were observed on a few photometric nights. The median seeing for the WMO

exposures was 1″.89. The standard processing pipeline for WMO data includes bias subtraction and flat fielding.

2.3. The Lick Nickel Telescope

The Lick 1 m Nickel reflector was used to observe Zw 229-015 during a few nights while KAIT was shut down for repairs. The Nickel Direct Imaging Camera contains a thinned, Loral 2048 × 2048 pixel CCD with a scale of 0″.184 pixel^{-1}, and the observations were obtained using 2 × 2 binning for the CCD readout. On one photometric night, Landolt (1992) standard-star fields were also observed. Overscan subtraction and flat fielding using twilight sky flats were done following standard procedures in IRAF.[19]

2.4. Maidanak Observatory

Zw 229-015 was observed on five nights in August and September using the Seoul National University 4096 × 4096 pixel camera (SNUCAM; Im et al. 2010) and *V*-band filter at the Maidanak Observatory 1.5 m telescope in Uzbekistan (Fairchild CCD; 0″.266 pixel^{-1}). The processing pipeline for SNUCAM data included overscan subtraction and flat fielding.

3. PHOTOMETRIC REDUCTIONS AND MEASUREMENTS

Our light-curve measurements followed the same procedures used by Walsh et al. (2009). First, each image was cleaned of cosmic-ray hits using the LA-COSMIC procedure (van Dokkum 2001) implemented in IRAF. Aperture photometry on Zw 229-015 and several comparison stars was performed using the IRAF task `phot`. Ultimately, six comparison stars were selected; these are illustrated in Figure 1. The photometric measurements were carried out with a range of aperture sizes. We found that the 4″ aperture radius gave the cleanest light curves, and our final photometry is based on this aperture size. The background sky annulus had inner and outer radii of 8″ and 14″.4. When more than one exposure was taken per night at a given telescope, the measurements were averaged together to give a single data point for that night.

Photometric calibration was accomplished by carrying out aperture photometry on the Landolt (1992) standard stars observed at WMO and the Nickel telescope on nights that were judged to be photometric by the observers. We used only *V*-band exposures and did not attempt to derive any color-dependent terms for the transformation between instrumental and calibrated *V* magnitudes. We found excellent agreement between the photometric calibrations for the night of September 26 at WMO and the night of August 12 at the Nickel telescope and took the average of the two calibrations to obtain our final photometric scale. Table 1 lists the positions and magnitudes of the six comparison stars.

The light curves from each telescope were separately normalized to *V*-band (Vega system) magnitudes based on the comparison-star photometry. To check for small systematic differences between the photometric scales of the four telescopes, which could be present because color terms were not measured, we determined the average offset between the KAIT and WMO light curves for the 53 nights when the object was observed at both telescopes. The weighted average offset was 0.010 ± 0.001 mag, and we applied this shift of 0.01 mag to the KAIT light curve as an empirical correction to bring it into agreement with the WMO photometric scale. Similar offsets of 0.010 and 0.020 mag were applied to the Nickel and Maidanak data points, respectively, in order to bring them into agreement with the combined KAIT and WMO light curve, based on the weighted average shift determined from nights when the galaxy was observed at more than one telescope.

The final light-curve data for Zw 229-015 are listed in Table 2. Some observations taken in cloudy conditions had very low signal-to-noise ratio (S/N), and we excluded any measurement having a formal uncertainty greater than 0.03 mag. We also discarded measurements from a few images that suffered from very poor flat fielding or other problems. The resulting light curve is illustrated in Figure 2.

The photometric uncertainties listed in Table 2 are the values returned by the photometry routine, which depend on photon-counting statistics for the object and background as well as on readout noise. These are likely to be underestimates of the true uncertainties, since additional errors can result from flat-fielding irregularities, point-spread function variations, and other issues. One way to estimate the actual photometric uncertainties is to examine the magnitude fluctuations in the comparison-star light curves, which are presumed to be intrinsically nonvariable. Comparison stars 3, 4, and 5 have *V* magnitudes very similar to that of Zw 229-015. For each of these stars, we examined the scatter of measurements about the mean magnitude and found standard deviations of 0.011–0.016 mag (see Table 1), while the median value of the formal photometric error on a single measurement for these stars is 0.006 mag. This discrepancy shows that the photon-counting statistics are usually not the dominant contributor to the error budget, except when the images have very low S/N. We address this issue by adding an additional

Table 1
Photometric Comparison Stars

Star	α (h:m:s)	δ (° :′:″)	*V* (mag)
1	19:05:19.49	42:28:57.7	14.983 ± 0.006
2	19:05:35.95	42:27:16.2	16.575 ± 0.014
3	19:05:33.71	42:28:50.5	15.954 ± 0.011
4	19:05:19.98	42:27:37.9	16.090 ± 0.016
5	19:05:27.28	42:26:48.8	16.000 ± 0.015
6	19:05:30.05	42:26:21.4	16.198 ± 0.016

Notes. Coordinates are J2000 and are based on an astrometric solution obtained using the astrometry.net package (Lang et al. 2010). The quoted magnitude uncertainties are calculated as the standard deviation of all measurements from KAIT and WMO for the complete light curve of each comparison star.

Table 2
Photometric Observations and Measurements

HJD−2450000	Telescope	*V* (mag)
5351.9785	K	15.989 ± 0.008
5352.8036	W	15.980 ± 0.003
5352.9688	K	15.976 ± 0.007
5353.9834	K	15.976 ± 0.009
5354.9619	K	15.957 ± 0.008

Note. Telescopes are listed as follows: K = KAIT, W = WMO, N = Lick Nickel, M = Maidanak.

(This table is available in its entirety in a machine-readable form in the online journal. A portion is shown here for guidance regarding its form and content.)

[19] IRAF is distributed by the National Optical Astronomy Observatory, which is operated by the Association of Universities for Research in Astronomy, Inc., under cooperative agreement with the National Science Foundation.

Table 3
Spectroscopic Observations and Measurements

UT Date	HJD−2450000	FWHM (arcsec)	S/N	$f(\mathrm{H}\alpha)$	$f(\mathrm{H}\beta)$	$f(\mathrm{H}\gamma)$	$f(\mathrm{H}\delta)$
				(10^{-15} erg cm^{-2} s^{-1})			
2010 May 19	5335.995	2.2	43	···	42.39 ± 0.24	18.27 ± 0.20	8.54 ± 0.18
2010 Jun 8	5355.978	2.1	45	184.52 ± 0.62	44.69 ± 0.25	20.44 ± 0.20	10.69 ± 0.19
2010 Jun 11	5358.954	2.9	37	190.32 ± 0.30	43.19 ± 0.32	19.56 ± 0.26	10.56 ± 0.25
2010 Jun 13	5360.985	2.5	40	190.51 ± 0.23	40.25 ± 0.27	17.76 ± 0.22	8.12 ± 0.21
2010 Jun 15	5362.928	2.7	40	181.04 ± 0.33	38.19 ± 0.29	17.04 ± 0.24	9.11 ± 0.22

Notes. The listed FWHM image quality is measured from the spatial profile of the bright star that fell on the spectrograph slit in each observation. The listed S/N is the signal-to-noise ratio per pixel in the reduced blue-side spectrum at $\lambda = 4700$ Å. Measured fluxes include the contribution of blended narrow-line components.

(This table is available in its entirety in a machine-readable form in the online journal. A portion is shown here for guidance regarding its form and content.)

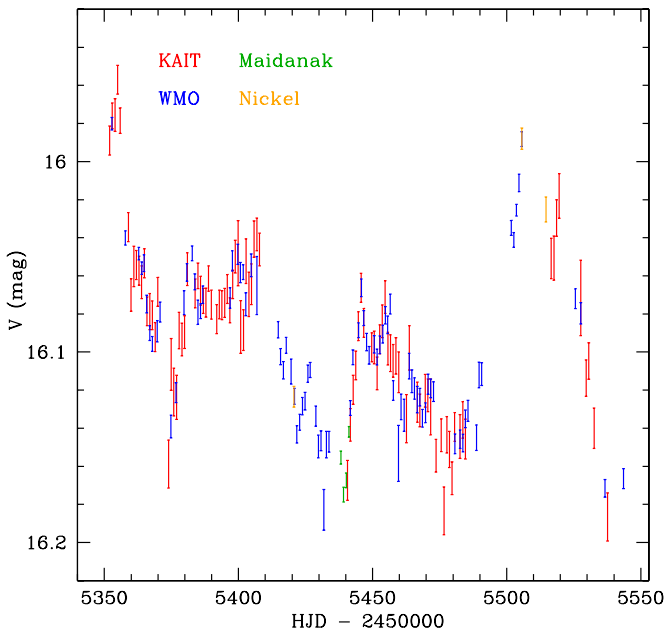

Figure 2. *V*-band light curve of Zw 229-015.
(A color version of this figure is available in the online journal.)

error term in quadrature to the photometric uncertainties prior to carrying out the cross-correlation measurements, as described in Section 6.

Our photometric aperture includes a substantial portion of the host galaxy, including essentially the entire bulge and much of the bar and disk. We do not attempt to subtract off this host-galaxy starlight contribution to the light-curve points, because our ground-based imaging does not have sufficiently high resolution to decompose the AGN point source and bulge into separate components. Removing this constant contribution of host-galaxy starlight would not affect the measurement of the reverberation lag.

A condensed version of the *V*-band light curve was prepared for the cross-correlation measurements by taking a weighted average of any photometric data taken within 5 hr of each other. This produces a light curve with at most one data point per night. The condensed light curve was then converted from magnitudes to linear flux units.

4. SPECTROSCOPIC OBSERVATIONS

The spectroscopic monitoring program at the Lick 3 m Shane telescope was carried out by several independent observing teams. Unlike other recent reverberation data sets that were obtained via long-duration, dedicated campaigns of classically scheduled observing nights, we chose to obtain synoptic monitoring of this single target by enlisting the entire community of observers using the Kast spectrograph at Lick during Summer and Fall 2010. The Kast spectrograph is mounted at the Cassegrain focus of the 3 m telescope for about half of each lunation, and the spectrograph is used for a variety of programs including supernova and transient follow-up observations, stellar spectroscopy, and AGN surveys. During each Kast observing night, the regularly scheduled observers took a 1200 s exposure of Zw 229-015 to contribute to this monitoring program. This strategy enabled us to collect a spectroscopic data set with almost nightly sampling during each dark run, except for weather-related losses. The spectroscopic monitoring began with one observation in May, and then continued with nightly observations during each dark run (weather permitting) from June through mid-December. From June through September, nearly every night was clear enough to observe, while October through December had more substantial weather losses, as is typical for Mt. Hamilton (the site of Lick Observatory). Table 3 gives a log of the Kast observations for the 54 nights when useful data were obtained. We have omitted data from two nights when Zw 229-015 was observed through very thick clouds, resulting in an S/N that was too low to be useful for any measurements.

Each observing team used a different instrumental setup for the spectrograph, designed for their primary science programs. On the blue side of the spectrograph, all observers used the 600-line grism, which gives a dispersion close to 1.0 Å pixel^{-1}. The spectral range falling on the blue-side detector is controlled by adjusting the CCD position via a manually movable stage, resulting in a fixed wavelength coverage for the entire night's observations. Most observing teams set the CCD to a position that covered ∼3440–5520 Å, placing the Hβ and [O III] $\lambda\lambda$4959, 5007 lines on the blue CCD. However, on several nights a bluer setup covering ∼3140–5150 Å or ∼3125–5135 Å was used, and with this setup the [O III] λ5007 line fell off the edge of the blue CCD, while the λ4959 line was still present.

For the red side of the spectrograph, several gratings are available and different gratings were installed on different nights. Since we could not ensure the same degree of consistency in the red-side observations as was obtained on the blue side, the red-side observations were a lower priority for this project. On some nights Zw 299-015 was not observed at all on the red side. When it was observed, gratings of 300, 600, and 1200 lines mm^{-1} were used for the red-side observations, with dispersions ranging from 1.2 to 4.6 Å pixel^{-1}. In most cases, the observers

used a d55 dichroic to separate the blue and red beams of the spectrograph, while on a few nights a mirror was used that directed all of the light to the blue side. When the 300 or 600 lines mm^{-1} gratings were used, there was usually a small region of wavelength overlap between the blue and red spectra. As a result of the heterogeneous nature of the red-side data, this paper focuses primarily on the analysis of the blue-side observations, which were all taken with the same grism and homogeneously observed except for the variations in spectral range described above.

With a single exception (the night of 2010 August 16), all observations of Zw 229-015 were obtained with the spectrograph slit at a position angle of P.A. = 56.°5. This angle was chosen so as to place a bright foreground star (marked with a square in Figure 1) in the slit, in order to aid in centering the primary target. A 4″ slit width was used for all exposures of Zw 229-015 and for the standard star BD+28°4211. A 1200 s exposure of Zw 229-015 and a 60 s exposure of BD+28°4211 were taken on most nights. On a few nights, the observers adjusted the exposure time due to weather constraints or took more than one exposure of the AGN. The airmass was smaller than 1.2 for 72% of the spectroscopic observations of Zw 229-015 and smaller than 1.5 for all but the final three exposures, when the object was observed at airmasses between 1.5 and 2.0. At the end of the observing season in December, when the target was observed at relatively high airmass, the fixed slit P.A. of 56.°5 was within 10°–20° of the optimal parallactic angle (Filippenko 1982) for the exposures, resulting in minimal differential light losses.

Table 3 also lists the "image quality," measured as the full width at half-maximum (FWHM) intensity of the spatial profile of the Galactic foreground star in the spectroscopic exposure. This image quality is primarily a measure of atmospheric seeing, but on some nights poor focus or occasional guiding errors added significantly to the spatial profile width. On clear nights, the blue-side observations typically resulted in an S/N per pixel of ∼40–45 in the extracted spectra at 4700 Å.

Dome-flat exposures and observations of arc-line lamps were taken during each afternoon. Dome flats were usually observed through a 2″ slit, since that slit width was used for the observers' primary programs. The difference in slit width between the AGN exposures and dome-flat exposures did not have any significant impact on the quality of the blue-side flattening, but on the red side it left strong fringing residuals at wavelengths longer than ∼7000 Å.

5. SPECTROSCOPIC REDUCTIONS AND MEASUREMENTS

Reduction of the Kast data followed standard procedures, including overscan subtraction, flat fielding, unweighted (nonoptimal) extractions, and wavelength calibration using the line-lamp exposures. An extraction width of 6.″5 was used. Flux calibration and a linear shift to the wavelength scale based on the wavelengths of night-sky emission lines were then applied to the spectra. The final blue-side spectra were binned to a uniform linear scale of 1 Å pixel^{-1}. Cosmic-ray residuals were removed from the reduced spectra by interpolation over the affected pixels. For nights when more than one exposure was taken, the multiple exposures were combined into a single reduced spectrum. Error spectra were also extracted and propagated through the full sequence of reductions. Figure 3 illustrates the reduced spectrum from a single observation.

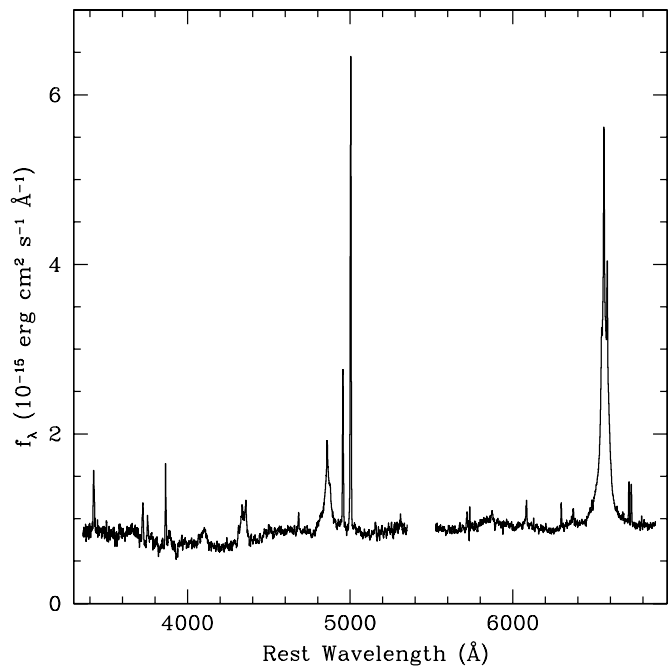

Figure 3. Combined Kast blue-side and red-side spectrum of Zw 229-015, from 2010-06-13. On the red side, a 1200 lines mm^{-1} grating was used, giving a dispersion of 1.2 Å pixel^{-1}.

We measured the centroid wavelength of the [O III] λ5007 line in each spectrum where the line was available. The median result is $\lambda_{\rm obs} = 5143.37 \pm 1.17$ Å, corresponding to an emission-line redshift of $z = 0.0273 \pm 0.0002$, consistent with the value from Falco et al. (1999). The fairly large dispersion in the [O III] wavelength measurements is most likely a result of variations in the centering of the AGN in the wide 4″ slit in each observation.

In order to intercalibrate the flux scales of the spectra and align them to a consistent wavelength scale, we employed the scaling procedure described by van Groningen & Wanders (1992), which is based on the assumption that the narrow [O III] emission-line flux is intrinsically constant over the timescale of the monitoring program. This method applies small wavelength shifts and a multiplicative flux scaling to each spectrum as well as a convolution with a Gaussian broadening kernel and finds the values of the shift, kernel width, and flux scaling factor that minimize the residual differences between the individual spectrum and a reference spectrum over a small wavelength region containing a narrow emission line and some surrounding continuum. According to van Groningen & Wanders (1992), their scaling method can yield accuracies of 5% or better, but higher accuracy (∼1%–2%) can be obtained with the best-quality data sets (e.g., Bentz et al. 2009; Denney et al. 2010). The flux scale of the reference spectrum was normalized by scaling it to match the mean [O III] λ5007 flux measured from eight nights that were considered to be photometric by the observers. For those eight nights, we find a mean observed [O III] λ5007 flux of 3.96×10^{-14} erg cm^{-2} s^{-1}, with a standard deviation of 4%, as measured from the flux-calibrated spectra prior to applying the scaling procedure.

When applying the van Groningen & Wanders (1992) procedure to the individual spectra, we used the [O III] λ4959 emission line as the flux scaling reference line, instead of the λ5007 line. The reason for this modification was that 10 of the spectroscopic observations used the blue-side CCD position that cut off the λ5007 emission line. The wavelength range in common to all

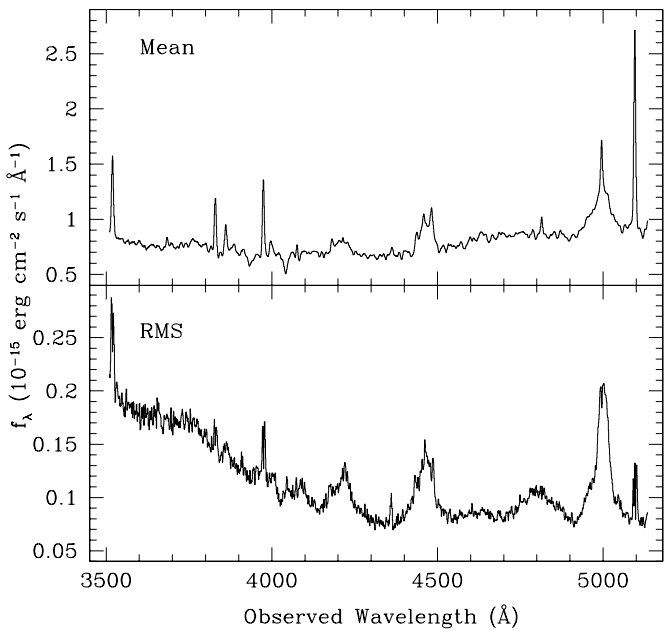

Figure 4. Mean and rms spectra. The plot illustrates the wavelength range in common to all of the blue-side spectra over the course of the campaign. Narrow emission-line residuals in the rms spectrum become stronger toward the blue end due to errors in wavelength calibration and differences in spectral focus between nights, since the spectral scaling optimizes the alignment and resolution of the spectra based on the λ4959 emission line at the red end of the blue-side spectra.

of the blue-side exposures extended to 5130 Å, including the λ4959 emission line and about 20 Å redward of the line. By using the λ4959 line as the flux reference, all of the spectra could be treated identically in the flux scaling procedure.

To examine the accuracy of the spectral scaling, we measured the flux in the λ4959 emission line from each spectrum after the scaling was applied, along with its uncertainty from the propagated error spectrum. We then determined the normalized excess variance σ_x^2 of the λ4959 light curve, following the definition used by Nandra et al. (1997):

$$\sigma_x^2 = \frac{1}{N\mu^2}\sum_{i=1}^{N}\left[(X_i-\mu)^2-\sigma_i^2\right], \quad (1)$$

where N is the total number of observations, μ is the mean flux, and X_i and σ_i are the individual flux values and their uncertainties. We find $\sigma_x = 0.024$, indicating that the residual errors in flux scaling contribute a spurious scatter to the light curves at the ∼2% level. These residuals are primarily due to seeing variations (particularly from the worst-seeing nights), miscentering of the target in the slit, and night-to-night variations in the telescope and spectrograph focus. Since Zw 229-015 exhibited dramatic, high-amplitude variability during the monitoring period, this residual scatter only has a small effect on the Hβ light curve.

Figure 4 illustrates the mean and root-mean-square (rms) spectra based on the full data set, constructed after applying the spectral scaling procedure to the data. The rms spectrum essentially gives the standard deviation of flux values at a given wavelength and illustrates the relative degree of variability of different wavelength regions of the spectrum. The broad Hβ, Hγ, and Hδ lines clearly stand out in the rms spectrum, and the variable continuum rises strongly toward the blue end of the observed wavelength range. In addition, a broad He II λ4686 line is evident in the rms spectrum, although it is too weak to be visible in the mean spectrum, where only the narrow component is clearly detected.

The flux scaling of the red-side data is more difficult to establish accurately. On the red side, there are no strong and isolated narrow emission lines, so the van Groningen & Wanders (1992) scaling routine cannot be applied directly. Additionally, on some nights the standard star was not observed simultaneously on the blue and red sides, resulting in flux scaling offsets when conditions were not photometric or the seeing was poor. In order to place the red-side data on a flux scale that was approximately consistent with the blue-side data, we first scaled each red spectrum by the scale factor used for the corresponding blue spectrum. This worked well for most nights, but left obvious offsets between the blue-side and red-side flux scales for a few nights. For those nights, an additional scaling factor was applied to the red-side data in order to bring the spectrum into agreement with the corresponding blue-side spectrum over the region of wavelength overlap or near-overlap. (We note that in a dedicated monitoring campaign with homogeneous observations, these flux scaling problems can be mitigated by using a spectrograph setup with substantial wavelength overlap between the red and blue sides and by observing standard stars simultaneously on both arms of the spectrograph.)

The Hβ light curve was measured by first subtracting a local, linear continuum underlying the line. The continuum-fitting windows were set to 4860–4910 Å and 5110–5130 Å. The Hβ flux was then measured by direct integration of the spectrum over 4930–5050 Å. We similarly measured the light curves of Hγ and Hδ. The emission-line summation windows for Hγ and Hδ were 4420–4500 Å and 4175–4245 Å, respectively, while the continuum windows were 4300–4400 Å and 4550–4600 Å for Hγ, and 4100–4150 Å and 4275–4325 Å for Hδ. On the red side, the emission-line window for Hα was 6600–6825 Å, and the continuum windows were 6500–6560 Å and 6940–7020 Å. All of these emission-line measurements include contributions from the narrow components of the Balmer lines, which are presumed to be nonvariable over the timescale of the monitoring project. In the mean spectrum, the narrow component of Hβ contributes ∼10% of the total Hβ flux. In addition, the Hγ integration window includes the [O III] λ4363 line, and the Hα window includes [N II] λλ6548, 6583. We do not attempt to decompose these emission blends into separate components.

Figure 5 displays the Balmer-line light curves. The Hβ light curve is the cleanest of the four, because of the proximity of the Hβ line to the [O III] line used as the flux scaling reference. The Hα light curve is substantially noisier than that of Hβ, despite the higher flux of Hα, due to the issues in matching the flux scales of the red-side and blue-side spectra. Nevertheless, all of the lines clearly show the same pattern of flux variations throughout the monitoring period.

The variability amplitude of the light curves can be quantified using the statistics R_{max} and F_{var} (e.g., Kaspi et al. 2000; Peterson et al. 2004; Bentz et al. 2009), where R_{max} is the ratio of maximum to minimum flux observed, and F_{var} is calculated according to

$$F_{var} = \frac{\sqrt{\sigma^2 - \langle\delta^2\rangle}}{\langle f\rangle}, \quad (2)$$

where σ^2 and $\langle\delta^2\rangle$ are the variance and the mean-square measurement uncertainty in the fluxes and $\langle f\rangle$ is the average flux in the light curve. For the Hβ light curve of Zw 229-015, we find $R_{max} = 2.68 \pm 0.04$ and $F_{var} = 0.23$. By both of these measures, Zw 229-015 displayed strong variability, exceeding

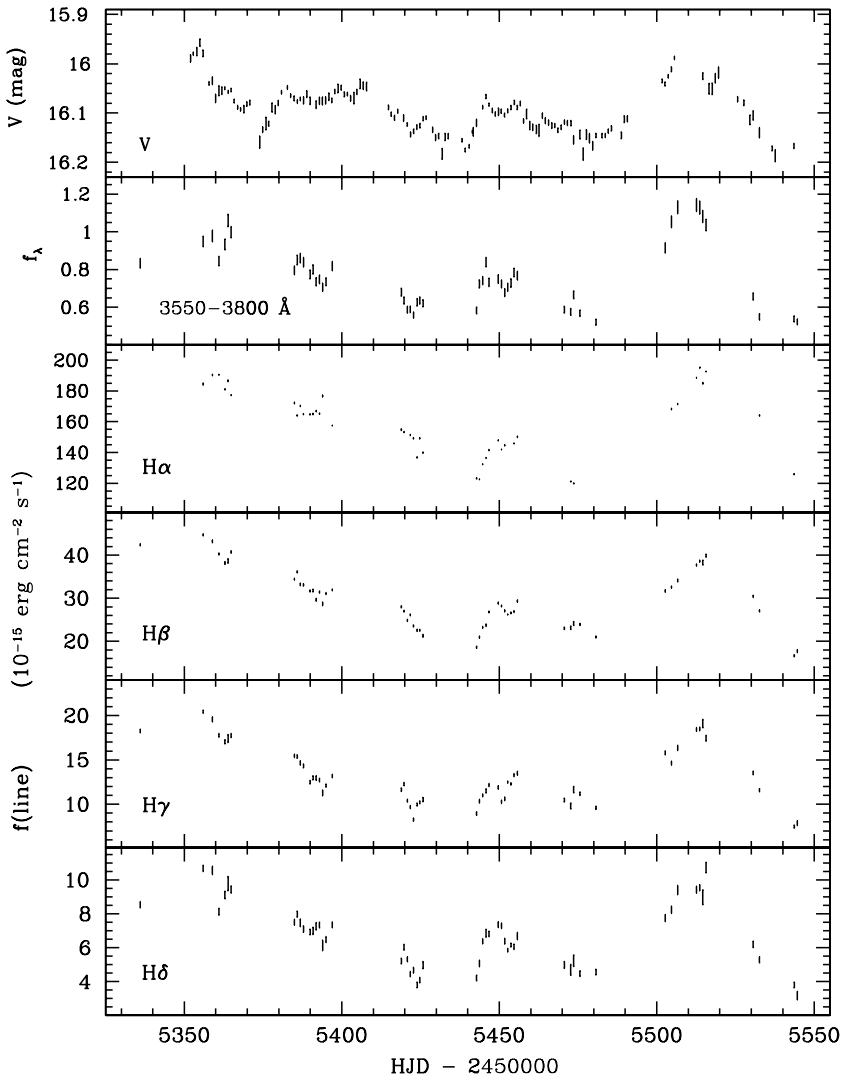

Figure 5. Light curves of the *V*-band continuum, the spectroscopic continuum over 3550–3800 Å (in units of 10^{-15} erg cm^{-2} s^{-1} Å^{-1}), and the Hα, Hβ, Hγ, and Hδ emission lines. The displayed *V*-band light curve is the "condensed" version in which measurements separated by less than 5 hr have been averaged together giving a single data point per night. The 3550–3800 Å continuum light-curve points are plotted with error bars of ±3% as a rough approximation of the uncertainties from the spectral scaling procedure and slit losses, since these errors dominate over photon-counting uncertainties.

the values of $R_{\rm max}$ and $F_{\rm var}$ observed for the entire sample of 13 AGNs observed in the 2008 Lick AGN Monitoring Project during a shorter two-month campaign (Bentz et al. 2009).

Figure 5 also displays the light curve of the continuum region 3550–3800 Å. (We refer to this spectroscopic *U*-band continuum measurement as the U_s light curve.) This is the region most dominated by the AGN continuum in the blue-side spectra. The spectroscopic continuum light curve is considerably noisier than the *V*-band light curve, as expected due to the combination of seeing-dependent slit losses, miscentering of the AGN in the slit, and the nonparallactic slit orientation. Nevertheless, the measurements illustrate that the *U*-band continuum generally follows the same pattern of variations as the *V*-band light curve, with a factor of ∼2 variability amplitude during the monitoring period.

6. REVERBERATION MEASUREMENTS

6.1. The Hβ Emission Line

Although it is difficult to see in Figure 5, the continuum and emission-line light curves do exhibit a small temporal offset. To demonstrate this more clearly, Figure 6 illustrates the central portion of the *V*-band continuum light curve (in flux units) and the Hβ light curve, after rescaling to approximately the same flux level. Aligning the two light curves by eye, it is evident that the Hβ variations lag the continuum by ∼4 days.

To determine the reverberation lag quantitatively, we employed the interpolation cross-correlation function (ICF) method (Gaskell & Peterson 1987), following the prescriptions described by White & Peterson (1994), Peterson et al. (2004), and Bentz et al. (2009). The ICF method deals with unevenly sampled time series by interpolating linearly between data points to obtain temporally matched time series for the continuum and emission-line light curves. For a given trial value of the lag time τ, the continuum light curve is shifted forward in time by τ days, and the cross-correlation is computed for the region of temporal overlap between the two light curves. The value of the cross-correlation function (CCF) for a given lag is computed twice: first by interpolating the shifted continuum light curve to the time steps of the emission-line light curve, and then by interpolating the emission-line light curve to the time steps of the shifted continuum light curve. The two interpolated versions

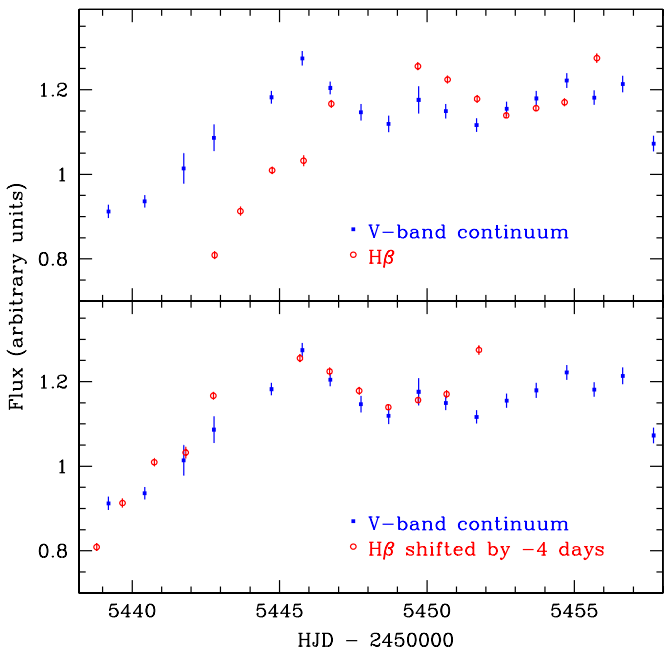

Figure 6. Central portion of the V-band continuum and Hβ light curves, illustrating the reverberation lag. The light curves have been scaled to the same overall flux level, and a constant offset was first subtracted from the continuum so that its variability amplitude would match that of the Hβ light curve. In the lower panel, the Hβ light curve is shifted by an offset of -4 days.

(A color version of this figure is available in the online journal.)

of the CCF are then averaged together to give the final CCF. We computed the CCF for lag values ranging from -20 to 30 days, in increments of 0.25 days.

Once the CCF is computed, the emission-line lag is determined in two ways: the peak of the CCF defines $\tau_{\rm peak}$, while the centroid of the CCF for points above 80% of the peak value of the CCF gives $\tau_{\rm cen}$. The value of $\tau_{\rm peak}$ and its uncertainty are quantized in units of the sampling interval used for the cross-correlation, in this case 0.25 days. Black hole masses from reverberation data are most often determined using $\tau_{\rm cen}$ (Peterson et al. 2004).

The final cross-correlation results and their uncertainties were determined by following the Monte Carlo bootstrapping procedure described by Peterson et al. (1998), Welsh (1999), and Peterson et al. (2004). In this method, a large number of modified realizations of the light curves are created and the CCF is computed for each realization of a pair of continuum and emission-line light curves. Each simulated light curve is generated by selecting n points randomly from the original light curve, where n is the number of points in the original light curve and the random selection allows a particular point to be chosen more than once. If a particular point is selected m times, then its uncertainty is reduced by a factor of $m^{1/2}$. Then, the simulated light curve is deviated by adding random Gaussian noise based on the uncertainty in each data point. The emission-line and continuum light curves are each resampled 10^4 times by this procedure, and for each pair of simulated light curves the CCF is determined. From these simulations, we build up distributions of values of $\tau_{\rm cen}$ and $\tau_{\rm peak}$. The final adopted values of $\tau_{\rm cen}$ and $\tau_{\rm peak}$ are defined to be the median values from each distribution. The 1σ uncertainty ranges on $\tau_{\rm cen}$ and $\tau_{\rm peak}$ are given by the range of lag values around the median that exclude the highest 15.87% and lowest 15.87% of lag values in the distribution.

When the continuum and emission-line light curves have very similar observational cadences, the two interpolated versions of the CCF are typically very similar in shape. However, if the two light curves have very different temporal sampling, then the two CCFs can differ substantially. As described by White & Peterson (1994), the two interpolated versions of the CCF are usually averaged together to obtain the final result, unless there is a strong reason to prefer one interpolation over the other. We tested whether this might affect the lag measurements by measuring $\tau_{\rm peak}$ and $\tau_{\rm cen}$ separately for the two interpolated versions of the CCF and comparing them with the results obtained for the averaged CCF. Although the two interpolated CCFs differed somewhat in shape, the measured lags were very similar in both cases, and the derived values of $\tau_{\rm cen}$ differed by only 0.18 days for the two separate CCFs. Given this close agreement, we chose to use the averaged CCF for our final results.

As discussed by Welsh (1999), the reliability of cross-correlation lag measurements can be improved by subtracting off any long-term secular variations from the light curves that occur on timescales much longer than the reverberation timescale. In practice, this is often accomplished by subtracting a simple linear fit from the light curves. We found that the measurements of $\tau_{\rm peak}$ and $\tau_{\rm cen}$ were virtually unchanged regardless of whether the light curves were linearly detrended, and detrending with a quadratic fit (in an attempt to remove the long-timescale curvature of the light curves) only modified the measured lags by less than their 1σ uncertainties. For our final measurements, we chose to use the linearly detrended light curves. We also tested to see whether the cross-correlation measurements would be affected by removal of the last few spectroscopic data points, during the period of poor weather when the sampling was very sporadic, and found that the results for $\tau_{\rm peak}$ and $\tau_{\rm cen}$ again were consistent with our final adopted values within the 1σ uncertainties.

As described above in Section 3, the photometric errors listed in Table 2 are likely to underestimate the true uncertainties. To account approximately for additional sources of error, we added 0.01 mag in quadrature to all of the V-band photometric errors prior to computing the cross-correlations. We found that this change had only a small effect on the cross-correlation results: the derived value of $\tau_{\rm cen}$ was either $3.85^{+0.62}_{-0.90}$ or $3.97^{+0.71}_{-0.93}$ days using the original photometric errors or the expanded error bars, respectively.

Our final measurement of the CCF gives observed-frame Hβ lags of $\tau_{\rm cen} = 3.97^{+0.71}_{-0.93}$ days and $\tau_{\rm peak} = 3.50^{+0.50}_{-0.75}$ days, consistent with the general expectation of a $\sim$4 day lag from inspection of the light curves (as in Figure 6). Converting to the rest frame of Zw 229-015, the lags are $\tau_{\rm cen} = 3.86^{+0.69}_{-0.90}$ and $\tau_{\rm peak} = 3.41^{+0.49}_{-0.73}$ days. All of the lag measurements are listed in Table 4. Figure 7 displays the autocorrelation function of the V-band light curve and the Hβ versus V-band CCF. The peak value of the CCF is 0.86, indicating a fairly strong correlation between the continuum and emission-line variations.

We also measured the Hβ lag relative to the U_s-band light curve and found observed-frame lags of $\tau_{\rm cen} = 5.16^{+1.27}_{-1.41}$ and $\tau_{\rm peak} = 3.25^{+2.75}_{-0.75}$ days. Within the substantial uncertainties, these results are consistent with the lag measurements carried out against the V band. Cross-correlating the V-band light curve against the U_s continuum, we find values of $\tau_{\rm peak}$ and $\tau_{\rm cen}$ that are consistent with zero within their 1σ uncertainties, so there is no significant detection of a lag between continuum bands. Higher-cadence observations would be needed in order

Table 4
Lag Measurements

Measurement	$\tau_{\rm cen}$ (days)	$\tau_{\rm peak}$ (days)
Hα vs. V	$5.22^{+0.83}_{-1.18}$	$4.75^{+1.00}_{-0.50}$
Hβ vs. V	$3.97^{+0.71}_{-0.93}$	$3.50^{+0.50}_{-0.75}$
Hγ vs. V	$3.46^{+0.80}_{-1.24}$	$2.50^{+0.75}_{-0.75}$
Hδ vs. V	$1.20^{+1.44}_{-1.69}$	$1.75^{+0.75}_{-0.50}$
Hβ vs. U_s	$5.16^{+1.27}_{-1.41}$	$3.25^{+2.75}_{-0.75}$
V vs. U_s	$0.89^{+1.44}_{-1.76}$	$-0.25^{+0.75}_{-0.50}$

Notes. All lags are in the observed frame. Rest-frame lags can be obtained by dividing by $1 + z$, or 1.0275 in this case. U_s denotes the U-band continuum measured from the blue-side spectra over 3550–3800 Å.

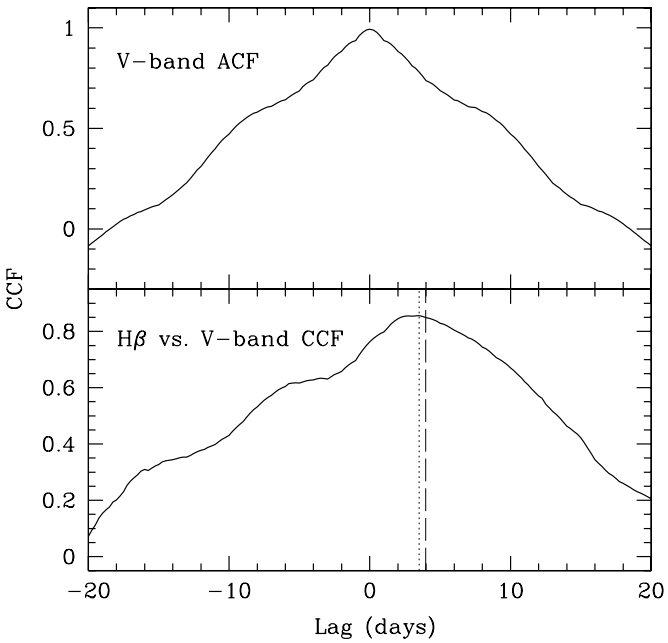

Figure 7. Top: autocorrelation function of the V-band light curve. Bottom: cross-correlation function of the Hβ and V-band light curves. The dotted and dashed lines mark the values of $\tau_{\rm peak}$ and $\tau_{\rm cen}$, respectively.

to search for any cross-band continuum lags (e.g., Sergeev et al. 2005). In addition to the featureless continuum of the AGN, the U_s spectral region also includes emission from the "small blue bump," which contains both Balmer continuum and Fe II emission. For NGC 5548, Maoz et al. (1993) showed that the small blue bump had a lag relative to the UV continuum that was similar to the lag of Lyα, consistent with the expectation that the small blue bump emission originates from the broad-line region (BLR). The nondetection of a lag between the U_s and V bands in Zw 229-015 suggests that either the small blue bump makes only a small contribution to the U_s band or that the Balmer continuum has an extremely short lag time relative to the primary continuum. The latter possibility would be consistent with the decreasing lags measured for higher-order Balmer lines (see Section 6.3 below).

There is a small contribution to the V-band flux from the broad Hβ line, and also an extremely small contribution from Hα at the red end of the Johnson V-filter passband. This can potentially bias the lag measurement, by adding a component to the continuum light curve that has zero temporal shift with respect to the emission-line light curve. Consequently, the lag measured from the cross-correlation peak will tend to be lower than the true lag. In order to assess the magnitude of this effect, we carried out synthetic photometry on Zw 229-015 using a combined blue-side and red-side spectrum constructed from a night with good overlap between the blue and red sides. Using the IRAF SYNPHOT package, we calculated the V-band magnitude of the spectrum twice: first on the original spectrum and then on a modified version of the spectrum in which the Hβ and Hα emission lines were completely removed by manually interpolating over them. The two synthetic V-band measurements differed by only 0.02 mag, indicating that the broad Balmer lines make only a very small contribution ($\sim$2%) to the broadband V magnitude.

To obtain a quantitative estimate of the magnitude of this bias on the lag measurement, we carried out a set of Monte Carlo simulations. We simulated a large number (10^4) of AGN light curves using the method of Timmer & Koenig (1995), for a power-density spectrum of the form $P(f) \propto f^{-2.5}$ normalized to a continuum rms variability of 20% over a 180 day period. A simple delta-function transfer function with a lag of 4 days was used to model the emission-line response to the continuum fluctuations. The "contaminated" V-band light curve was simulated by adding the emission-line light curve to the continuum light curve, weighted so that 2% of the total flux was from the emission-line contribution. With each set of simulated light curves we measured the emission-line lag relative to the uncontaminated continuum light curve and relative to the continuum light curve with the added emission-line contribution.

The simulations confirm that the bias in the lag measurements is very small for Zw 229-015. When the emission-line contribution to the continuum light curve is at the observed 2% level as in Zw 229-015, the simulations show that the measurement of $\tau_{\rm cen}$ is biased on average by only -0.07 days (with an rms scatter of 0.05 days in the bias for the full ensemble of simulations), relative to the measurement obtained by cross-correlating against the pure continuum light curve. For Zw 229-015, the bias is much smaller than the overall uncertainty in the lag measurement, but it can become significant for higher levels of emission-line contamination. We carried out additional simulations and found that if the emission-line contribution to the broadband light curve increases to 10%, for example, the average bias in the $\tau_{\rm cen}$ measurement is -0.3 days (for the same model parameters described above). For future reverberation campaigns that use broadband photometry to measure the continuum light curves, it will be important to carry out simulations like these to assess the likely magnitude of this effect on each individual object. The size of the bias would depend on both the emission-line equivalent width and on the target's redshift, since higher redshifts would move the broad Hβ line closer to the peak transmission of the V filter. Alternatively, another approach would be to subtract off the emission-line flux directly from the broadband light curve before measuring the cross-correlation lag.

6.2. Velocity-resolved Measurements

The behavior of the reverberation lag as a function of velocity across broad emission lines is dependent on the kinematics of the BLR, and recent ground-based programs have successfully obtained velocity-resolved measurements of reverberation lags for Hβ and other lines in several AGNs (Kollatschny 2003; Bentz et al. 2009, 2010a; Denney et al. 2010). Our Zw 229-015 data set is not ideally suited for velocity-resolved reverberation measurements, because the Hβ lag is fairly short and the

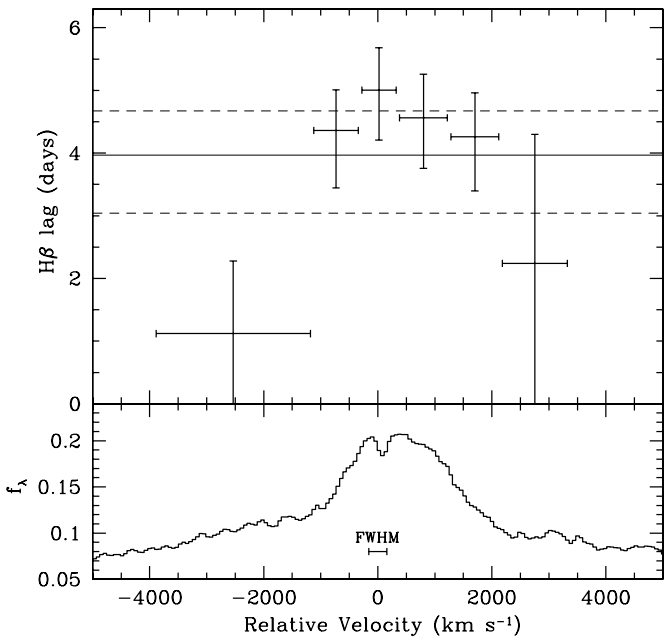

Figure 8. Velocity-resolved reverberation results for Hβ. The lower panel shows the rms line profile on a velocity scale, and the error bar illustrates the FWHM instrumental broadening of 313 km s^{-1}. The upper panel shows the value of $\tau_{\rm cen}$ measured in six velocity bins, and the horizontal error bars denote the size of each velocity bin. The solid and dashed lines mark the value of $\tau_{\rm cen}$ for the entire Hβ line and its 1σ uncertainty range.

monthly gaps in the spectroscopic light curve limit the measurement accuracy for lags of individual velocity segments of the Hβ line.

Nevertheless, we are still able to obtain some rudimentary information on the velocity dependence of the reverberation lag across the Hβ line profile. Light curves were measured for several independent velocity segments across the Hβ line, and the individual segment light curves were cross-correlated against the *V*-band continuum. The results are illustrated in Figure 8. Six velocity segments were used for the final measurements. In the line wings, where the variability amplitude is relatively low, the measurements have large uncertainties; the lags measured for the blue-wing and red-wing segments are consistent with zero within their 1σ uncertainties. (We used a broader velocity segment for the blue wing because subdividing the blue wing into even smaller segments led to very poor cross-correlation results, with some subsegments having negative lags.)

With these caveats in mind, the velocity-resolved behavior seen in Figure 8 shows marginal evidence for a slightly longer lag in the line core relative to the mean lag, while the lag in the line wings is shorter. A symmetric blue–red response in the velocity-delay map, with shorter lags in the line wings, is qualitatively consistent with Keplerian motion of the BLR clouds (e.g., Welsh & Horne 1991), but due to the large uncertainties in the velocity-resolved measurements we refrain from drawing any specific conclusions about the BLR kinematics. The results do illustrate that Zw 229-015 is a promising candidate for further velocity-resolved reverberation work. Given the strong and rapid variability in this object, a high-cadence monitoring campaign could obtain much better results, and a reconstruction of the two-dimensional transfer function (i.e., the distribution of lag time as a function of velocity) might be obtainable (e.g., Bentz et al. 2010b).

6.3. Reverberation Lags of Hα, Hγ, and Hδ

We measured cross-correlation lags for the other Balmer lines following the same methods that were used for Hβ, including the linear detrending. The Balmer-line reverberation lags follow the same pattern found previously for other AGNs, where the Hα line has the longest lag and higher-order Balmer lines have progressively shorter lags (e.g., Kaspi et al. 2000; Bentz et al. 2010a). The lag of Hδ is too small to be resolved significantly, and our measurement of $\tau_{\rm cen}$ indicates a 1σ upper limit of $\tau_{\rm cen} < 2.6$ days. As discussed by Bentz et al. (2010a), this trend in Balmer-line lags is the result of the differences in optical depths for the Balmer lines in the BLR, and the same behavior is seen in BLR photoionization models (Korista & Goad 2004). For example, the Hα line has the highest total optical depth through the BLR, and the observed Hα emission originates primarily from larger radii in the BLR where the optical depth is smaller. Using the $\tau_{\rm cen}$ measurements, we find a ratio of Balmer-line reverberation lags of τ(Hα):τ(Hβ):τ(Hγ) = 1.31:1.00:0.87, which is within the range observed by Bentz et al. (2010a) for AGNs having similar emission-line lags of a few days.

6.4. Hβ Line Width

Virial estimates of black hole masses based on reverberation-mapping data employ the width of broad emission lines to give the typical velocity for BLR gas. Following procedures often employed for reverberation-mapping data (e.g., Peterson et al. 2004), we measured the FWHM and the line dispersion (or second moment) of the Hβ line from both the mean and the rms spectra. In both cases, a linear continuum was fitted to regions on either side of the Hβ line, and then subtracted off. The FWHM was measured directly from the continuum-subtracted line profile, and the line dispersion $\sigma_{\rm line}$ (in velocity units) was calculated as

$$\sigma_{\rm line}^2 = \left(\frac{c}{\lambda_0}\right)^2 \left(\left[\sum \lambda_i^2 S_i\right] \Big/ \left[\sum S_i\right] - \lambda_0^2\right), \qquad (3)$$

where S_i is the flux density at wavelength bin λ_i and λ_0 is the flux-weighted centroid wavelength of the line profile.

While the narrow component of Hβ essentially vanishes in the rms spectrum, it must be removed from the mean spectrum before the broad-line width can be measured. The narrow [O III] λ4959 emission line has a nearly Gaussian profile with FWHM = 6.6 Å, and we used this as a model to subtract off the narrow component of Hβ. To determine the final values and uncertainties for the line widths, we followed the Monte Carlo method described by Peterson et al. (2004) and Bentz et al. (2009), creating randomly resampled realizations of the mean and rms spectra. To construct each realization, we randomly selected 54 spectra from our data set, without regard to whether an individual spectrum was already selected, and then determined the mean and rms spectra for that randomly sampled set. For a total of 1000 realizations, we measured FWHM and $\sigma_{\rm line}$ for Hβ, from both the mean and rms spectra. In each realization, the borders of the continuum-fitting windows were shifted randomly over a range of 10 Å in order to account for the line-width uncertainty resulting from the specific choice of continuum regions. The final value and uncertainty for each line-width measurement (FWHM and $\sigma_{\rm line}$) are taken to be the median value and standard deviation determined from the full ensemble of simulations. From the rms spectrum, we measure FWHM = 2280 ± 65 km s^{-1} and $\sigma_{\rm line}$ = 1600 ± 47 km s^{-1}

for Hβ. The mean spectrum gives FWHM $= 3360 \pm 72$ and $\sigma_{\rm line} = 1645 \pm 16$ km s^{-1} for the broad Hβ line. After removal of the narrow component from the mean spectrum, the broad Hβ line centroid in the observed frame is $\lambda_0 = 4993.2$ Å. The redshift inferred from the broad Hβ line is therefore 0.0271, and there is no significant velocity offset between the narrow [O III] line and the broad Hβ emission.

The observed line widths are affected by instrumental broadening in the 4″ wide slit, but only by a very small amount. The instrumental line width adds in quadrature to the observed line width (as in $\sigma^2_{\rm observed} = \sigma^2_{\rm intrinsic} + \sigma^2_{\rm instrumental}$, or similarly for the FWHM values). We can obtain an upper limit to the instrumental broadening by measuring the widths of arc-lamp lines observed through the 4″ slit, since the arc lamps uniformly illuminate the entire slit width while the AGN does not (at least under typical seeing conditions). From the Cd I line at 5086 Å, we find an upper limit to the instrumental broadening of FWHM$_{\rm inst} < 7.7$ Å, corresponding to an instrumental velocity width of FWHM$_{\rm inst} < 454$ km s^{-1} or an instrumental dispersion of $\sigma_{\rm inst} < 193$ km s^{-1}. This instrumental broadening is small enough that the maximum possible contribution of instrumental broadening to the observed $\sigma_{\rm line}$ of the broad Hβ line is only 0.9% of the observed line dispersion.

To estimate the likely value of the instrumental dispersion $\sigma_{\rm inst}$, we followed the method described by Bentz et al. (2009), using an observation of [O III] through a narrower slit to determine the intrinsic width of the line. The initial test spectrum of Zw 229-015, taken on 2010 April 18, was observed through a 2″ slit. In that exposure, the [O III] λ5007 line has a raw FWHM of 5.44 Å, and the 5086 Å arc line has FWHM $=$ 4.18 Å. Assuming that the AGN nearly fills the slit in the 2″ observation (roughly the size of the seeing disk), this implies an intrinsic line width of FWHM $= 203$ km s^{-1} for [O III]. The instrumental broadening for the 4″ slit can then be estimated as the difference in quadrature between the observed width of [O III] in the 4″ slit (FWHM $= 373$ km s^{-1}) and the intrinsic [O III] width measured from the 2″ observation. This implies an instrumental contribution of FWHM$_{\rm inst} = 313$ km s^{-1} or $\sigma_{\rm inst} = 133$ km s^{-1} for the 4″ slit, consistent with the upper limits derived previously.

The corresponding corrections to the measured broad Hβ line width for this instrumental broadening are very small. From the rms spectrum, the corrected Hβ widths are FWHM $= 2260 \pm 65$ km s^{-1} and $\sigma_{\rm line} = 1590 \pm 47$ km s^{-1}, and in the mean spectrum the corrected Hβ widths are FWHM $= 3350 \pm 72$ and $\sigma_{\rm line} = 1640 \pm 16$ km s^{-1}.

7. THE MASS OF THE BLACK HOLE

Measurements of reverberation lag and broad-line width can be combined to give an estimate of black hole mass, under the assumption that the line width is primarily due to virial motion of broad-line gas (e.g., Gaskell 1988; Kaspi et al. 2000; Peterson et al. 2004). From the virial theorem, we have

$$M_{\rm BH} = f\frac{(c\tau)(\Delta V)^2}{G}, \quad (4)$$

where τ is the reverberation lag and $(c\tau)$ gives the mean radius of the BLR, ΔV is some measure of the broad-line width in velocity units (typically either FWHM or the line dispersion σ), and f is a scaling factor which is dependent on the geometry and kinematics of the BLR as well as our viewing angle. Since these parameters of the BLR are unknown, it has become customary to use a single value for f that should ideally represent the mean value of the virial normalization factor for an appropriate ensemble of AGNs. The adopted value of f can be based either on some set of assumptions about BLR kinematics (e.g., Kaspi et al. 2000) or by finding the normalization that brings reverberation-mapped AGNs into best agreement with the local $M_{\rm BH}$–σ relation of quiescent galaxies (Onken et al. 2004; Woo et al. 2010).

For consistency with the majority of recent reverberation work, we use $\sigma_{\rm line}$(Hβ) measured from the rms line profile as the measure of ΔV and $c\tau_{\rm cen}$(Hβ) as the measure of BLR size; these parameters have been shown to yield the most robust mass estimates (Peterson et al. 2004). For the virial normalization factor, we use $f = 5.25$, derived from the full available sample of reverberation-mapped AGNs having measured stellar velocity dispersions (Woo et al. 2010). Combining the rest-frame value $\tau_{\rm cen} = 3.86^{+0.69}_{-0.90}$ with $\sigma_{\rm line} = 1590 \pm 47$ km s^{-1}, we obtain a "virial product" of $(c\tau)(\Delta V)^2/G = 1.91^{+0.36}_{-0.46} \times 10^6\ M_\odot$. Applying the virial normalization factor $f = 5.25$, this gives an estimated black hole mass of $M_{\rm BH} = 1.00^{+0.19}_{-0.24} \times 10^7\ M_\odot$.

We note that the quoted uncertainties on $M_{\rm BH}$ above only include the propagated errors on the lag and line-width measurements, but not the (unknown) systematic uncertainty on the applied value of f. From examination of the scatter of reverberation-mapped AGNs about the best-fitting $M_{\rm BH}$–σ relation, the typical uncertainty in the value of f applied to any individual AGN is probably at the level of a factor of $\sim$3 (e.g., Onken et al. 2004; Woo et al. 2010), so the actual error in the estimated value of $M_{\rm BH}$ is dominated by the uncertainty in f and not by the measurement errors in the Hβ lag or width. A long-term goal of reverberation-mapping work is to use velocity-resolved measurements to directly constrain the BLR geometry and kinematics so that accurate black hole masses can be derived for individual AGNs, but such analysis is beyond the scope of this work.

We can estimate the Eddington ratio $L/L_{\rm Edd}$ for Zw 229-015 using the V-band continuum flux and a bolometric correction. Without high-resolution optical images or an accurate model of the stellar population, we cannot directly determine the amount of starlight contamination to the V-band magnitudes or spectroscopic continuum fluxes, but a rough approximation will suffice to estimate $L/L_{\rm Edd}$. According to the extinction map of Schlegel et al. (1998), the Galactic foreground extinction toward Zw 229-015 is $A_V = 0.24$ mag. We make the simplifying assumption that the extinction correction and starlight contamination correction would roughly compensate for each other and take the rest-frame 5100 Å flux density from the mean spectrum as an estimate of the intrinsic (extinction-free) AGN flux density. We find $\lambda f_\lambda(5100\ \text{Å}) = 4.2 \times 10^{-12}$ erg s^{-1} cm^{-2} in the mean spectrum, corresponding to $\lambda L_\lambda(5100\ \text{Å}) = 7.1 \times 10^{42}$ erg s^{-1} for a luminosity distance of 119 Mpc (assuming *WMAP-7* cosmological parameters with $H_0 = 71$ km s^{-1} Mpc^{-1}; Larson et al. 2011). Applying the same bolometric correction used by Peterson et al. (2004) of $L_{\rm bol} = 9 \times \lambda L_\lambda(5100\ \text{Å})$, we obtain an estimated $L_{\rm bol} = 6.4 \times 10^{43}$ erg s^{-1} and $L/L_{\rm Edd} \approx 0.05$. This value is within the typical range found for nearby reverberation-mapped Seyferts (Peterson et al. 2004).

The possible influence of radiation pressure on black hole masses derived from reverberation mapping has been the subject of much recent discussion (Marconi et al. 2008, 2009; Netzer 2009; Netzer & Marziani 2010). The impact of radiation pressure on the motion of BLR clouds is likely to be strongest for AGNs radiating at high luminosity, but Zw 229-015 has a

rather modest Eddington ratio and any corrections for radiation pressure should be relatively minor. Marconi et al. (2008) proposed a modification to the virial equation, adding a term proportional to the AGN continuum luminosity, as in

$$M_{\rm BH} = f\frac{(c\tau)(\Delta V)^2}{G} + g\frac{L_{5100}}{10^{44}\,{\rm erg\,s^{-1}}}, \quad (5)$$

where $L_{5100} = \lambda L_\lambda$ at 5100 Å, and where the numerical value of f differs from the value used to normalize the "standard" virial equation (Equation (4)). Using the sample of reverberation-mapped AGNs having measured stellar velocity dispersions, they estimated best-fit values of $f = 3.1$ and $\log g = 7.6$. Applying this formalism to Zw 229-015, we obtain an estimate of $M_{\rm BH} \approx 8.8 \times 10^6\ M_\odot$ for Zw 229-015. This value is lower than the pure virial estimate for $M_{\rm BH}$, due to the combination of the smaller f value derived by Marconi et al. (2008) and the relatively low luminosity of Zw 229-015, but it differs from the pure virial estimate by only 12%, or less than 1σ. From examination of the orbits of BLR clouds under the influence of radiation pressure, Netzer & Marziani (2010) proposed an alternative variant of the virial equation as a new mass estimator, dependent on the AGN continuum luminosity and broad-line FWHM. Applying their mass estimator (their Equation (18)) and using FWHM(Hβ) measured from the mean spectrum, we obtain $M_{\rm BH} \approx 1.25 \times 10^7\ M_\odot$ for Zw 229-015. In either case, the corrections to $M_{\rm BH}$ for radiation-pressure effects are not very large, and they are far smaller than the overall uncertainty in the value of the virial normalization factor f for an individual AGN.

8. DISCUSSION AND CONCLUSIONS

This data set was obtained using a somewhat unconventional strategy, in which the spectroscopic observations were done on a nightly basis, but only during the dark runs. We find that this method can deliver high-quality reverberation results, provided that a well-sampled photometric light curve (not having large gaps) is also obtained. Since there are many facilities that can deliver nightly, queue-scheduled imaging observations without monthly gaps, this is now a straightforward approach to measurement of long-term light curves and reverberation lags for additional AGNs. In terms of the measurement accuracy for the Hβ lag, our results for Zw 229-015 are similar in quality to what was obtained for several objects with similar lag times of a few days during the 2008 Lick AGN Monitoring Project (Bentz et al. 2009), a program comprising 64 mostly consecutive nights of spectroscopic observations along with nightly photometry.

Our results demonstrate that Zw 229-015 will be an excellent target for a variety of future investigations. Its strong and rapid variability is noteworthy in comparison to many other objects having similar black hole masses and luminosities (e.g., Bentz et al. 2009), and it is very fortunate that such a nearby and highly variable AGN happens to be in the *Kepler* field of view. While the *Kepler* light curve for Zw 229-015 is not yet available, we anticipate that it will enable fundamentally new investigations into the properties of AGN optical continuum variability. There are only a few other low-redshift Seyfert galaxies being monitored by *Kepler*, and although their variability properties are currently unknown, it seems likely that Zw 229-015 will be the most important object of this small sample. As such, it is crucial that Zw 229-015 continue to be monitored by *Kepler* for the longest possible duration during the mission.

Additional observations of Zw 229-015 can be used to measure the galaxy's bulge properties, to place it on the correlations between black hole mass and bulge luminosity or mass, and to add it to the sample used to calibrate the relationship between BLR radius and continuum luminosity following the methods described by Bentz et al. (2006). Similarly, a measurement of the bulge velocity dispersion for Zw 229-015 can be used to add this galaxy to the $M_{\rm BH}$–σ relation for reverberation-mapped AGNs (Nelson et al. 2004; Onken et al. 2004; Woo et al. 2010). Our wide-slit observations are not well suited to carrying out measurements of stellar kinematics, but stellar absorption features including the Ca II triplet absorption lines are easily visible in the Lick spectra, so it should be straightforward to measure the bulge velocity dispersion with suitable new observations. Other observing programs for Zw 229-015 are currently in progress, including near-infrared monitoring with *Spitzer* to measure the dust reverberation timescale. We will also revisit our Hβ reverberation measurement when the *Kepler* light curve becomes available, since the sampling and precision of the *Kepler* data may lead to an improved determination of the emission-line lag.

To summarize our conclusions, we have measured a rest-frame reverberation lag of $\tau_{\rm cen} = 3.86^{+0.69}_{-0.90}$ days for the Hβ line in Zw 229-015. Combining this result with the broad Hβ line width, we obtain a virial estimate of $\sim 10^7\ M_\odot$ for the black hole in this galaxy, under the assumption of a virial normalization factor of $f = 5.25$. The mass estimate does not change significantly if we adopt the method of Marconi et al. (2008) to obtain a mass estimate corrected for the dynamical influence of radiation pressure in the BLR. The *Kepler* target Zw 229-015 is destined to be one of the most important AGNs for investigations of the origin and characteristics of optical continuum variability. As recent observations have begun to reveal connections between optical continuum variability characteristics and black hole masses in AGNs, this estimate of $M_{\rm BH}$ will be a valuable asset for future interpretation of the *Kepler* light curve for Zw 229-015.

Research by A.J.B., M.L.N., and J.L.W. at UC Irvine has been supported by NSF CAREER grant AST–0548198. A.V.F.'s group is grateful for the financial support of NSF grant AST–0908886, the TABASGO Foundation, Gary and Cynthia Bengier, and the Richard and Rhoda Goldman Fund; also, J.M.S. thanks Marc J. Staley for a Graduate Fellowship. KAIT and its ongoing operation were made possible by donations from Sun Microsystems, Inc., the Hewlett-Packard Company, AutoScope Corporation, Lick Observatory, the NSF, the University of California, the Sylvia & Jim Katzman Foundation, and the TABASGO Foundation. The West Mountain Observatory 0.9 m telescope has been supported by NSF grant AST–0618209. M.D.J., C.D.L., E.G.H., and J.W.M. thank the Department of Physics and Astronomy at Brigham Young University for continued support of research efforts at the West Mountain Observatory. Tommaso Treu's research group at UCSB has been supported by NSF CAREER grant NSF–0642621 and a Packard Fellowship. Research by J.H.W. has been supported by the Basic Science Research Program through the National Research Foundation of Korea funded by the Ministry of Education, Science and Technology (2010-0021558). We thank Rick Edelson for discussions that motivated this project. We are grateful to the Lick Observatory staff for their assistance in obtaining the spectroscopic observations, and to the staff of the Maidanak Observatory for obtaining data for this project. We also thank Tabitha Buehler, Carl Melis, Dovi Poznanski, X. Prochaska, and

Ben Zuckerman for contributing observations. This research has made use of the NASA/IPAC Extragalactic Database (NED) which is operated by the Jet Propulsion Laboratory, California Institute of Technology, under contract with NASA.

REFERENCES

Bentz, M. C., Peterson, B. M., Pogge, R. W., Vestergaard, M., & Onken, C. A. 2006, ApJ, 644, 133
Bentz, M. C., et al. 2009, ApJ, 705, 199
Bentz, M. C., et al. 2010a, ApJ, 716, 993
Bentz, M. C., et al. 2010b, ApJ, 720, L46
Borucki, W. J., et al. 2010a, Science, 327, 977
Borucki, W. J., et al. 2010b, ApJ, 713, L126
Collier, S., & Peterson, B. M. 2001, ApJ, 555, 775
Denney, K. D., et al. 2010, ApJ, 721, 715
Falco, E. E., et al. 1999, PASP, 111, 438
Filippenko, A. V. 1982, PASP, 94, 715
Filippenko, A. V., Li, W. D., Treffers, R. R., & Modjaz, M. 2001, in ASP Conf. Ser. 246, IAU Colloq. 183, Small Telescope Astronomy on Global Scales, ed. B. Paczynski, W.-P. Chen, & C. Lemme (San Francisco, CA: ASP), 121
Gaskell, C. M. 1988, ApJ, 325, 114
Gaskell, C. M., & Peterson, B. M. 1987, ApJS, 65, 1
Im, M., Ko, J., Cho, Y., Choi, C., Jeon, Y., Lee, I., & Ibrahimov, M. 2010, J. Korean Astron. Soc., 43, 75
Kaspi, S., Smith, P. S., Netzer, H., Maoz, D., Jannuzi, B. T., & Giveon, U. 2000, ApJ, 533, 631
Kelly, B. C., Bechtold, J., & Siemiginowska, A. 2009, ApJ, 698, 895
Kollatschny, W. 2003, A&A, 407, 461
Korista, K. T., & Goad, M. R. 2004, ApJ, 606, 749
Landolt, A. U. 1992, AJ, 104, 340
Lang, D., Hogg, D. W., Mierle, K., Blanton, M., & Roweis, S. 2010, AJ, 139, 1782
Larson, D., et al. 2011, ApJS, 192, 16
MacLeod, C. L., et al. 2010, ApJ, 721, 1014
Maoz, D., et al. 1993, ApJ, 404, 576
Marconi, A., Axon, D. J., Maiolino, R., Nagao, T., Pastorini, G., Pietrini, P., Robinson, A., & Torricelli, G. 2008, ApJ, 678, 693
Marconi, A., Axon, D. J., Maiolino, R., Nagao, T., Pietrini, P., Risaliti, G., Robinson, A., & Torricelli, G. 2009, ApJ, 698, L103
Markowitz, A., et al. 2003, ApJ, 593, 96
McHardy, I. M., Koerding, E., Knigge, C., Uttley, P., & Fender, R. P. 2006, Nature, 444, 730
Nandra, K., George, I. M., Mushotzky, R. F., Turner, T. J., & Yaqoob, T. 1997, ApJ, 476, 70
Nelson, C. H., Green, R. F., Bower, G., Gebhardt, K., & Weistrop, D. 2004, ApJ, 615, 652
Netzer, H. 2009, ApJ, 695, 793
Netzer, H., & Marziani, P. 2010, ApJ, 724, 318
Onken, C. A., Ferrarese, L., Merritt, D., Peterson, B. M., Pogge, R. W., Vestergaard, M., & Wandel, A. 2004, ApJ, 615, 645
Peterson, B. M., Wanders, I., Horne, K., Collier, S., Alexander, T., Kaspi, S., & Maoz, D. 1998, PASP, 110, 660
Peterson, B. M., et al. 2004, ApJ, 613, 682
Proust, D. 1990, IAU Circ., 5134, 2
Schlegel, D. J., Finkbeiner, D. P., & Davis, M. 1998, ApJ, 500, 525
Sergeev, S. G., Doroshenko, V. T., Golubinskiy, Y. V., Merkulova, N. I., & Sergeeva, E. A. 2005, ApJ, 622, 129
Timmer, J., & Koenig, M. 1995, A&A, 300, 707
Uttley, P., McHardy, I. M., & Papadakis, I. E. 2002, MNRAS, 332, 231
van Dokkum, P. G. 2001, PASP, 113, 1420
van Groningen, E., & Wanders, I. 1992, PASP, 104, 700
Voges, W., et al. 1999, A&A, 349, 389
Walsh, J. L., et al. 2009, ApJS, 185, 156
Welsh, W. F. 1999, PASP, 111, 1347
Welsh, W. F., & Horne, K. 1991, ApJ, 379, 586
White, R. J., & Peterson, B. M. 1994, PASP, 106, 879
Woo, J.-H., et al. 2010, ApJ, 716, 269
Zimmermann, H.-U., Boller, T., Döbereiner, S., & Pietsch, W. 2001, A&A, 378, 30